

Supplementary Materials for
**Organocatalyzed Atroposelective Dynamic Kinetic Resolutions via
Transient Seven-Membered Cyclic Hemiacetals**

Qinglong Zhou *et al.*

*Corresponding author: Xing Yang, xingyang@hunnu.edu.cn; Xinglong Zhang, xinglong.zhang@cuhk.edu.hk;
Yonggui Robin Chi, robinchi@ntu.edu.sg.

This PDF file includes:

Supplementary Text
Table S1 to S4
Figure S1 to S7
References

combined organic layer was dried over anhydrous Na₂SO₄, evaporated under reduced pressure. Then, the mixture was purified by column chromatography using silica gel (PE/EA = 10:1) to afford the crude products (including hemiacetals) **1f**, **1i**, **1k**, **1n**, **1o**.

Section S4. Mechanism studies

Computational methods for mechanism studies

Geometry optimizations in the gas phase were initially carried out using global hybrid functional M06-2X (79) with Karlsruhe-family basis set of double- ζ valence def2-SVP (86, 87) for all atoms as implemented in *Gaussian 16* rev. A.03. (88) Minima and transition structures on the potential energy surface (PES) were confirmed as such by harmonic frequency analysis, showing respectively zero and one imaginary frequency, at the same level of theory.

Single point (SP) corrections were performed using M06-2X functional and def2-TZVP (86) basis set for all atoms. The implicit SMD continuum solvation model was used to account for the solvent effects of dichloroethane (DCE) on the overall free energy PES. Gibbs energies were evaluated at the room temperature, as was used in the experiments, using a quasi-RRHO treatment of vibrational entropies. (89, 90) Vibrational entropies of frequencies below 100 cm⁻¹ were obtained according to a free rotor description, using a smooth damping function to interpolate between the two limiting descriptions. The free energies were further corrected using standard concentration of 1 mol/L, which was used in solvation calculations. SMD(DCE)-M06-2X/def2-TZVP//M06-2X/def2-SVP Gibbs energies are given and quoted in kcal mol⁻¹ throughout. *Unless otherwise stated, these solvent-corrected values are used for discussion throughout the main text and in this supporting information.*

Non-covalent interactions (NCIs) were analyzed using NCIPLOT calculations. The .wfn files for NCIPLOT were generated at M06-2X/def2-SVP (86, 87) level of theory. NCI indices calculated with NCIPLOT were visualized at a gradient isosurface value of $s = 0.5$ au. These are colored according to the sign of the second eigenvalue (λ_2) of the Laplacian of the density ($\nabla^2\rho$) over the range of -0.1 (blue = attractive) to $+0.1$ (red = repulsive). All molecular structures and molecular orbitals were visualized using *PyMOL* software. (91)

Model reaction

For this study, we select the model reaction depicted in Figure S1 for mechanistic studies using DFT modeling.

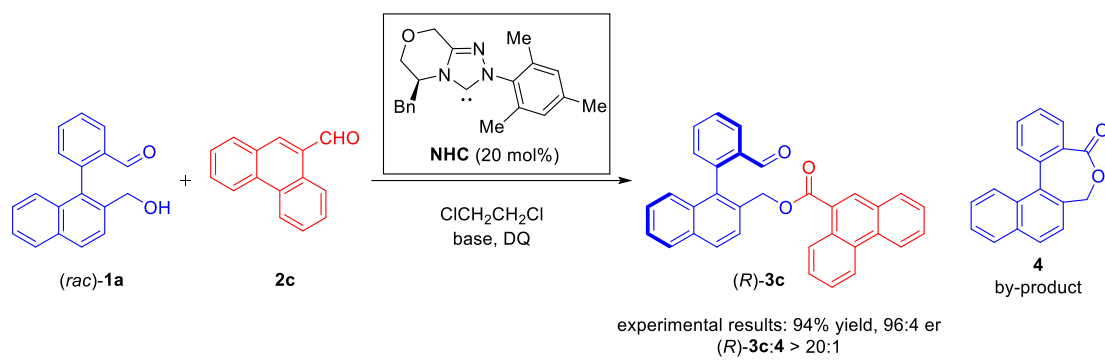


Figure S1. Model reaction used for DFT based mechanistic studies.

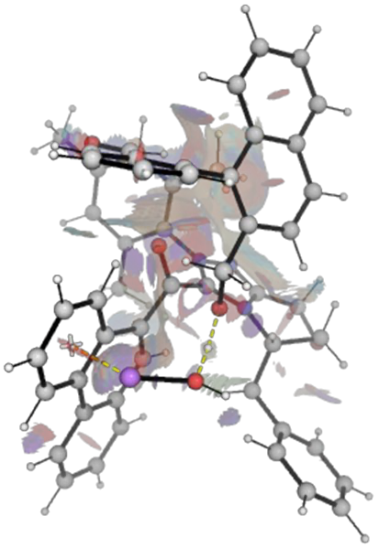
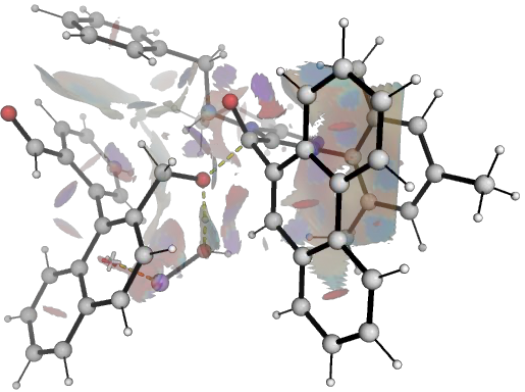
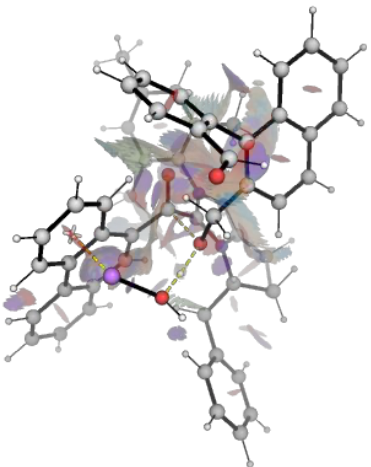
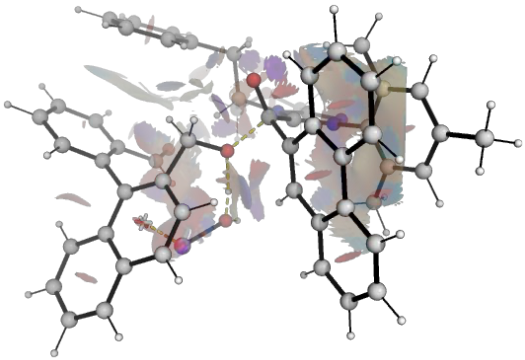

TS-<i>R-Re</i>	TS-<i>R-Si</i>
$\Delta\Delta G^\ddagger = 3.5$ kcal/mol	$\Delta\Delta G^\ddagger = 0.0$ kcal/mol
	
TS-<i>S-Re</i>	TS-<i>S-Si</i>
$\Delta\Delta G^\ddagger = 2.9$ kcal/mol	$\Delta\Delta G^\ddagger = 3.5$ kcal/mol
	
	

Figure S2. NCI plots for the enantio-determining TSs for the NHC catalyzed model reaction.

Distortion-interaction analysis for enantio-determining TSs

Distortion-interaction analysis is applied to enantio-determining TSs (**TS-*R-Si*** and **TS-*S-Re***) to discern the factors affecting enantioselectivity. The transition state structures are decomposed by dividing the cationic acyl azolium intermediate **II** (formed from NHC and **2c**), and substrate **1a** with LiOH as components. Single point calculations with SMD(DCE) solvent correction were applied performed at M06-2X/def2-TZVP level of theory to obtain distortion and interaction energies. The distortion energy is given by:

$$E_{dist} = E_{TS,frag1} + E_{TS,frag2} - (E_{eq,frag1} + E_{eq,frag2})$$

where $TS,frag1,2$ represent individual fragments in their distorted transition state geometries; and $eq,frag1,2$ represent individual fragments in their optimized, equilibrium ground-state geometries; the interaction energy is given by:

$$E_{int} = E_{TS} - (E_{TS,frag1} + E_{TS,frag2})$$

which accounts for the stabilizing interactions (e.g., electrostatic, orbital, dispersion) between the distorted fragments in the TS.

Thus, the total activation energy is given by:

$$\Delta E^\ddagger = E_{dist} + E_{int}.$$

Note that this single point activation energy and the activation energy differences $\Delta\Delta E^\ddagger$ between the TSs (**TS-*R-Si*** vs. **TS-*S-Re***) may be different from the Gibbs energy differences $\Delta\Delta G^\ddagger$ that is computed fully (including vibrational frequencies analysis) at SMD(DCE)-M06-2X/def2-TZVP//M06-2X/def2-SVP level of theory.

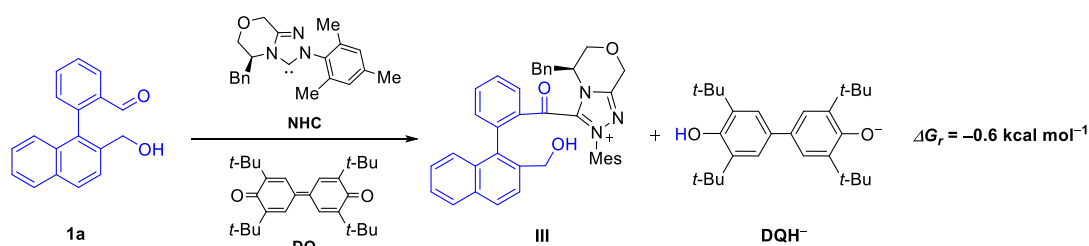
The analysis gives a $\Delta\Delta E^\ddagger$ (TS) of 3.4 kcal/mol in favor of **TS-*R-Si*** over **TS-*S-Re***. Although **TS-*R-Si*** exhibits a lower stabilizing interaction energy over **TS-*S-Re*** ($E_{int} = -112.6$ vs. -127.3 kcal/mol), this is outweighed by its significantly lower distortion energy ($E_{dist} = 83.2$ vs. 101.3 kcal/mol), Table S4. As a result, the overall ΔE^\ddagger for **TS-*R-Si*** is 3.4 kcal/mol lower than that of **TS-*S-Re*** (-29.4 vs. -26.0 kcal/mol), rendering **TS-*R-Si*** the more favorable transition state, Table S4.

Table S4: Distortion-interaction analysis.

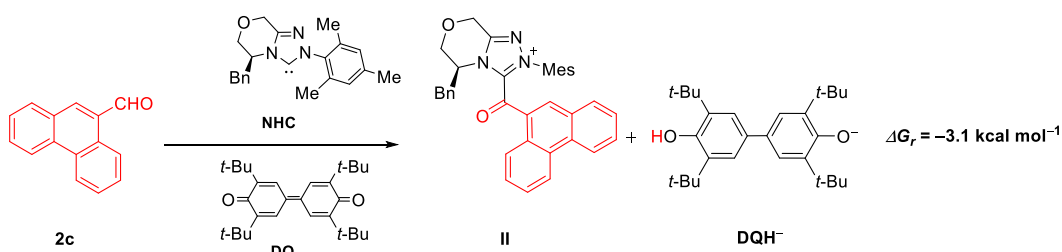
Transition State	ΔE^\ddagger	E_{dist}	E_{int}
TS-<i>R-Si</i>	-29.4	83.2	-112.6
TS-<i>S-Re</i>	-26.0	101.3	-127.3

Model reactions for the formation of acyl azolium intermediates II and III

a)



b)

**Figure S3.** Model reactions employed for DFT based estimation of the reaction free energies for the formation of a) III, and b) II.**Interconversion of *R* and *S* forms of **1a'** and **4****

To estimate the free energy barrier for the interconversion of *R* and *S* forms of intermediate **1a'**, we employed two diastereoisomeric conformers differing at the chiral carbon center as starting geometries for dihedral rotation around the C–C bond in **1a'**, which led to the identification of transition states **TS-rot-1** and **TS-rot-2** (Figure S4a). The calculated barrier for **TS-rot-1** is 19.9 kcal/mol, which is 2.7 kcal/mol lower than that of **TS-rot-2** (22.6 kcal/mol). Similarly, the computed free energy barrier for the interconversion of *R* and *S* forms of compound **4**, via **TS-rot-4** (Figure S4b), is 22.2 kcal/mol, in excellent agreement with the experimentally determined value of 21.9 kcal/mol. This consistency supports the reliability of our computed rotational barrier for intermediate **1a'**, which could not be measured

experimentally, and suggests that it falls in a similar range of value (~ 20 kcal/mol).

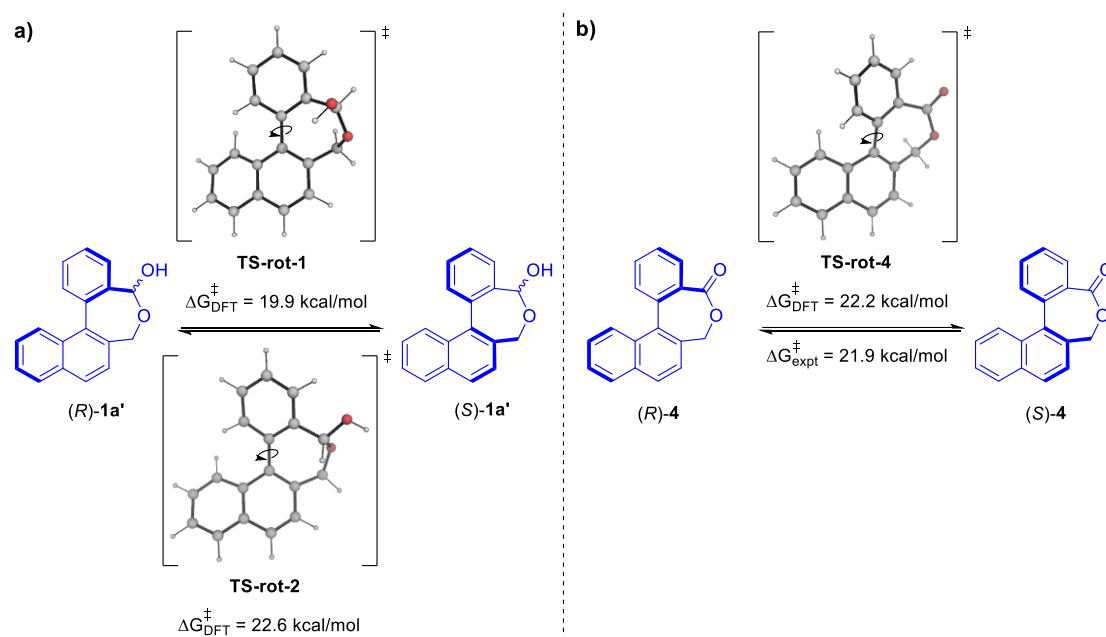


Figure S4. Interconversion of *R* and *S* forms of a) intermediate **1a'** and b) compound **4** via rotational transition state over the C–C axial axis.

Interconversion of *R* and *S* forms of substrate **1a**

We studied the rotational barriers for the enantiomerization of substrate **1a**. Initially, we carried out a relaxed PES scan of a dihedral angle along the axial C–C bond using M06-2X/def2-SVP level of theory in the gas phase (Figure S5). Our results indicate that the highest energy structures for enantiomerization (structures 2 and 5, Figure S5) are lying at ~ 36 kcal/mol and ~ 56 kcal/mol, respectively. Subsequently, using these highest energy structures as initial guess structures for TS search, we successfully located the *true* TS structures for enantiomerization via rotation along the axial C–C bond. The computed barriers are 34.8 kcal/mol for **TS-rot-1a** (Figure S6), which is the rotational barrier for the aldehyde group to cross over the naphthalene side group, and 36.0 kcal/mol for **TS-rot-1b** (Figure S6), which is the rotational barrier for the aldehyde group to cross over the benzyl alcohol group. Both rotational TSs have very high barriers, indicating that direct enantiomerization of **1a** is unlikely under ambient reaction conditions. However, a lower energy pathway involving the conversion of **1a** firstly to lactol intermediate **1a'** (Figure S4a) and then its rotation about the axial C–C bond of **1a'** may enable the overall enantiomerization of **1a** via the intermediary of **1a'**.

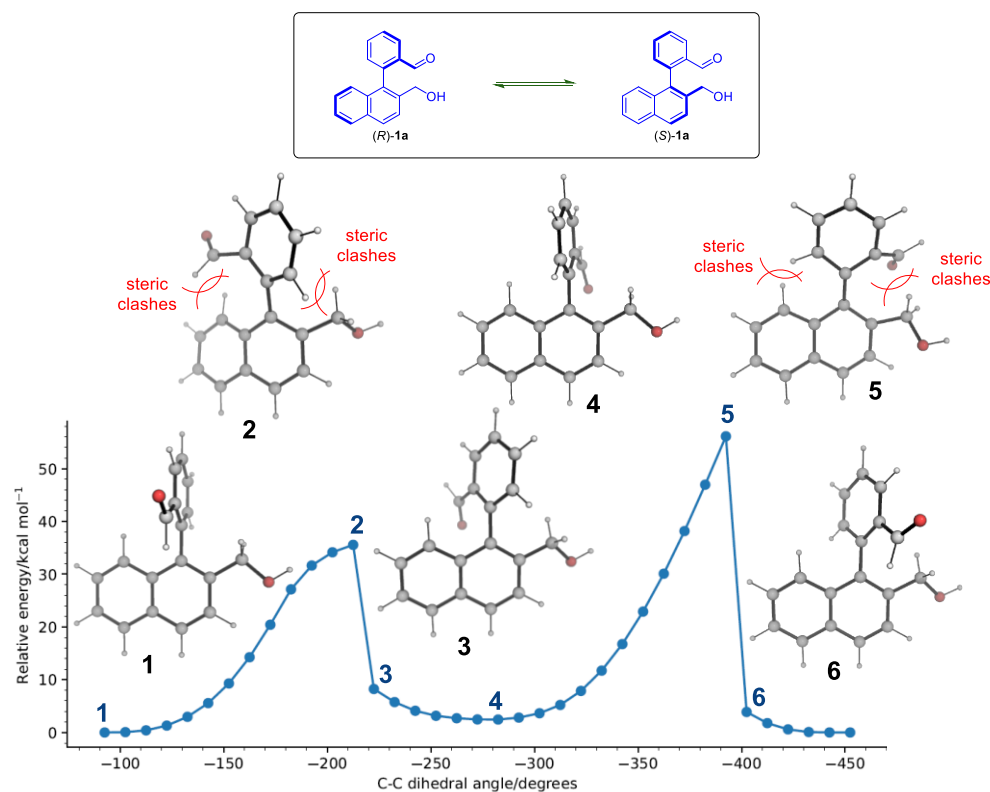


Figure S5. Relaxed potential energy surface (PES) scan for the dihedal angle along the C–C axial bond of the substrate 1a, computed at M06-2X/def2-SVP level of theory.

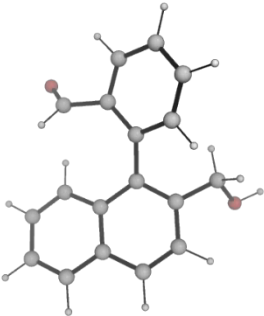
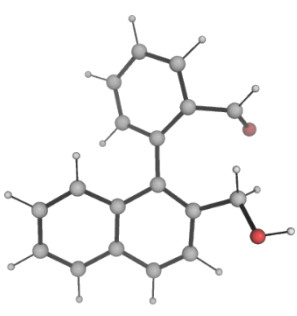
TS-rot-1a	TS-rot-1b
$\Delta G^\ddagger = 34.8$ kcal/mol	$\Delta G^\ddagger = 36.0$ kcal/mol
	

Figure S6. DFT-optimized rotational TS structures for the enantiomerization of substrate 1a, TS-rot-1a and TS-rot-1b. Rotational barriers are calculated at SMD(DCE)-M06-2X/def2-TZVP//M06-2X/def2-SVP level of theory at room temperature and are given in kcal mol⁻¹.

Optimized structures and raw energies

Geometries of all optimized structures (in .xyz format with their associated energy in Hartrees) are included in a separate folder named *DFT_optimized_structures*. All these data have been deposited and uploaded to <https://zenodo.org/records/15774233> (DOI: 10.5281/zenodo.15774233).

Absolute values (in Hartrees) for SCF energy, zero-point vibrational energy (ZPE), enthalpy and quasi-harmonic Gibbs free energy (at 298.15K) for gas-phase M06-2X/def2-SVP optimized structures are given below. Single point corrections in SMD dichloroethane using M06-2X/def2-TZVP functional are also included.

Structure	E/au	ZPE/au	H/au	T.S/au	qh-G/au	SP MN15/def2- TZVP
NHC	-1052.302228	0.405003	-1051.874	0.075513	-1051.94366	-1053.501437
1a	-843.825362	0.273106	-843.534948	0.059848	-843.591925	-844.783629
2c	-652.108964	0.20644	-651.89008	0.047376	-651.936711	-652.8426641
R-3a	-1494.78425	0.460964	-1494.294624	0.087758	-1494.375325	-1496.459919
4	-842.656882	0.2542	-842.387955	0.05225	-842.439156	-843.6087804
DQ	-1240.022914	0.620195	-1239.369317	0.091886	-1239.456033	-1241.422698
DQH ⁺	-1240.720581	0.629463	-1240.057724	0.090543	-1240.143811	-1242.179491
LiOH	-83.270079	0.012644	-83.253346	0.014279	-83.267625	-83.40038398
II	-1703.66235	0.604815	-1703.023396	0.096538	-1703.113329	-1705.620376
III	-1895.390031	0.673552	-1894.677632	0.105227	-1894.775689	-1897.561404
TS-R-Re	-2630.855321	0.893829	-2629.907483	0.138275	-2630.034388	-2633.846465
TS-R-Si	-2630.860919	0.894017	-2629.912509	0.139815	-2630.040674	-2633.851275
TS-S-Re	-2630.850654	0.893342	-2629.902844	0.141124	-2630.031256	-2633.845822
TS-S-Si	-2630.862383	0.895464	-2629.912954	0.137461	-2630.03982	-2633.847948
R-1a'	-843.840012	0.277324	-843.547328	0.053242	-843.599581	-844.7929473
TS-rot-1	-843.800491	0.277187	-843.505079	0.06163	-843.565415	-844.7558681
TS-rot-2	-843.802331	0.27673	-843.510774	0.052133	-843.561952	-844.7569107
TS-rot-1a	-843.768686	0.273675	-843.479129	0.054341	-843.532574	-844.7309058
TS-rot-1b	-843.767694	0.273508	-843.478442	0.053767	-843.531481	-844.7290457
TS-1a	-1896.145788	0.681982	-1895.42506	0.104971	-1895.52298	-1898.276139
TS-2c	-1704.425354	0.613712	-1703.77692	0.098736	-1703.86817	-1706.339554
TS-rot-4	-842.623597	0.253801	-842.35582	0.050299	-842.405519	-843.573727